

Enhanced fatigue performance and surface mechanical properties of AISI 304 stainless steel induced by electropulsing-assisted ultrasonic surface rolling process

Hai-bo Wang

Advanced Materials Institute, Graduate School at Shenzhen, Tsinghua University, Shenzhen 518055, People's Republic of China

Xin-hua Yang and He Li

School of Materials Science and Engineering, Dalian Jiaotong University, Dalian 116028, People's Republic of China

Guo-lin Song and Guo-yi Tang^{a)}

Advanced Materials Institute, Graduate School at Shenzhen, Tsinghua University, Shenzhen 518055, People's Republic of China

(Received 14 May 2018; accepted 10 August 2018)

The evolution of fatigue performance and surface mechanical properties of AISI 304 stainless steel induced by the electropulsing-assisted ultrasonic surface rolling process (EP-USRP) was systematically investigated by integrating instrumented indentation, scanning electron microscopy with electron backscatter diffraction, and transmission electron microscopy. The results indicate that higher hardness, greater strength, finer ultra-refined grains, and higher residual compressive stress are formed within the strengthened layer compared with the original ultrasonic surface rolling process (USRP). EP-USRP with the optimized experimental parameters can produce a higher average rotating bending fatigue strength for AISI 304 stainless steel than USRP. Anomalously and noteworthy, all fatigue specimens treated by EP-USRP showed an incomplete fracture, revealing a higher reservation of safety in practical engineering applications. The further modified structure strengthening and stress strengthening induced by EP-USRP are likely the primary intrinsic reasons for the observed phenomena. Furthermore, the influence mechanism of EP-USRP was discussed scrupulously.

I. INTRODUCTION

Fatigue performance of a metallic material is strongly dependent on its surface conditions, such as surface roughness, microcrack, residual stress, and microstructure within the surface layer.^{1–3} In general, the fatigue damage of a metal component begins with the minor defect on the surface, which ultimately leads to the failure of the component.^{4,5} Therefore, the effective surface strengthening engineering techniques are imperative to improve the surface properties of a metallic material, especially which working under the action of an alternating load.^{6,7}

The electropulsing-assisted ultrasonic surface rolling process (EP-USRP), a novel surface strengthening technology for metallic materials, shows a broad prospect in engineering application.⁸ EP-USRP utilizes the combination of structure strengthening and stress strengthening induced by severe plastic deformation (SPD) in the ultrasonic surface rolling process (USRP) and the

modification and optimization of microstructure produced by electropulsing treatment.^{2,9,10} In EP-USRP, an ultra-hard processing tip is used to roll the material surface under a static force, and the dynamic impact is applied to the surface through the tip supplied by ultrasonic apparatus in the normal direction. Meanwhile, electropulsing is exerted in the plastic deformation area. Therefore, with the help of electropulsing and compared with USRP, the further modified changes are achieved on the material surface in EP-USRP, which are confirmed in the following forms: higher surface hardness, ultra-refined grains, effective surface crack healing, and greater impact depth, which can make metallic materials with gradually surface strengthened layer and a better engineering performance.^{2,8}

In our previous research, the changes of surface mechanical properties and the microstructure of AISI 304 stainless steel induced by EP-USRP were studied superficially in a traditional way.⁹ In the present work, the evolution of surface mechanical properties, particularly the fatigue performance of AISI 304 stainless steel induced by EP-USRP, is investigated profoundly. Based on careful experiment research, a model describing the

^{a)}Address all correspondence to this author.

e-mail: tanggy@sz.tsinghua.edu.cn

DOI: 10.1557/jmr.2018.307

evolution of fatigue performance of AISI 304 stainless steel induced by EP-USRP is proposed, and the influence mechanism is discussed scrupulously.

II. EXPERIMENTAL DETAILS

A. Materials

Commercial solution annealed AISI 304 stainless steel rods were cut into pole-shaped samples and then processed by turning to the specimens with a dimension of $\Phi 16.8$ mm \times 150 mm and a axial surface roughness of Ra 0.8 μ m to maximize the uniformity of surface morphology characteristics. The chemical composition of the as-received AISI 304 stainless steel is presented in Table I.

B. Experimental procedures

Basic mechanism principle demonstration of EP-USRP is depicted in Fig. 1. The USRP and EP-USRP experiments were carried out on a self-built platform based on a conventional lathe. An ultra-hard scrollable rolling tip with a hardness of 80 HRC, surface roughness of Ra 0.1 μ m, and a radius of curvature of 7 mm attached to an ultrasonic apparatus is used to roll the material surface under a static force. A dynamic impact is applied to the surface through the tip supplied by an ultrasonic apparatus in the normal direction. Meanwhile, electropulsing with a sharp waveform was exerted in the plastic deformation area by using a self-designed power generator.⁹ Therefore, with the synergism of electropulsing, the repeated, high-frequency strikes cause SPD on the material surface, which leads to refined grains and residual compressive stresses at and below the material surface to a certain depth that depends on the amplitude, static force, strike rate, current intensity, frequency, etc. In the present work, the basic parameters were as follows: rolling line speed was 24 m/min, feeding rate was 0.1 mm/rev, static force was 950 N, ultrasonic vibration amplitude was 8 μ m, ultrasonic vibration frequency was 30 kHz, and repeated processing number was 5. The electropulsing parameters are given in Table II. For each EP-USRP experiment, electropulsing was used through the entire process, whilst the ultrasonic impact treatment was started up only when the surface temperature of the specimen reached an equilibrium value. The surface temperature of the specimen was monitored by using a K-type surface thermocouple, and the results are shown in Table II. L-G 8 guide rail oil was used in the process of cooling and lubricating.

C. Microstructural characterization

A Hitachi S4800 scanning electron microscope (SEM) (Hitachi, Ltd., Tokyo, Japan) was utilized to analyze the fatigue fracture surface and cross-sectional microstructure within the surface strengthened layer. An FEI Nova NanoSEM 450 (FEI Company, Hillsboro, Oregon) equipped with a Hikari Plus detector was used to obtain electron backscatter diffraction (EBSD) (EDAX Inc., Mahwah, New Jersey). A JEM-3200FS transmission electron microscope (TEM) (JEOL Ltd., Tokyo, Japan) was utilized to analyze the refined microstructure and obtain corresponding selected area electronic diffraction within the strengthened layer.

D. Mechanical property tests

1. Hardness test

The hardness within the strengthened layer was measured by using a G200 instrumented indentation system (with xp basic method) attached with a Berkovich indenter with a maximum load of 30 gf, 30 s loading time, and 15 s holding time. Poisson's ratio of the specimen was adopted as 0.3. An average of 10 parallel measurements was used for each reported data point.

2. Residual stress

In the instrumented indentation test, the average contact pressure equals to the hardness of the material that we want to test. It is unaffected by any pre-existing tensile or residual compressive stress, and this statement is substantiated by theoretical reasoning and finite element analyses as well as experiments.¹¹ But the indented penetration depths of the materials which have the same hardness level in the instrumented indentation test are affected directly by pre-existing residual stress states.¹¹ Thus, the residual stress can be estimated from the difference of the indenter penetration depths between the specimen without residual stress and the specimen with a residual stress that we want to measure; here the used two specimens have the same hardness level. The present work adopted the method introduced by Suresh et al. for estimating residual stress of the treated specimen by instrumented sharp indentation. The reference specimen without residual stress was prepared by stress relief annealing a corresponding specimen which has a residual stress and the same hardness level in the muffle furnace at 550 $^{\circ}$ C for 1.5 h followed by furnace cooling. Due to the incomplete stress release for AISI 304 stainless steel under

TABLE I. Chemical component of the as-received commercial annealed AISI 304 stainless steel rods.

Chemical elements	C	Cr	Co	Cu	Ni	Mn	Mo	N	P	S	Si	Fe
Content/wt%	0.019	18.39	0.16	0.40	8.56	1.40	0.35	0.081	0.033	0.024	0.21	Bal.

the given experimental conditions, the calculated value of residual compressive stress was relatively smaller than the real one, inversely for residual tensile stress was relatively larger than the real value, theoretically.

3. True stress–true strain curve, yield strength, and strain-hardening exponent test

The dimensional analysis of instrumented indentation has been carried out to obtain the local elastic–plastic properties quantitatively in the past few years frequently.^{12–17} It can provide the basic relations between the elastic–plastic properties of the indented materials, which were obtained from their indentation load–penetration depth measurements.¹² Dao et al. performed a parametric study of 76 cases with various elastic–plastic parameters using finite element analysis and found that the loading curvature can be normalized independent of the strain-hardening exponent at the representative strain of 0.033.¹⁷ Based on this, they established a set of dimensionless functions that can predict the indentation response from the elastic–plastic properties. The present work adopted the reverse analysis method introduced by Dao et al. for determining the plastic properties of materials treated by USRP and EP-USRP. Beginning from that, the distributions of yield strength, strain hardening exponent, and true stress–true strain curve within the surface strengthened layer were calculated concurrently. Here, each group specimens were set as

three parallel tests for obtaining average measuring results, and the uniaxial stress–strain relation of AISI 304 stainless steel was estimated by the power law constitutive equation legitimately.

4. Fatigue test

Three kinds of specimens used in the fatigue test were as follows: specimens processed by mechanical polishing with an axial surface roughness of R_a 0.2 μm , specimens processed by USRP with R_a at 0.2 μm , and specimens processed by EP-USRP at 600 Hz with R_a at 0.2 μm . The rotating bending fatigue tests were carried out using a PQ-6 rotating bending fatigue test machine. The loading profile was a sine function and the frequency was 50 Hz and the stress ratio was -1 . The targeted life of the specimen was adopted as 10^7 , and the fatigue strength was evaluated by up-and-down method. All tests were carried out at ambient temperature and with a water-cooled environment.

III. RESULTS

A. Cross-sectional nanoindentation hardness and residual stress gradient distributions within the strengthened layer

Generally, the specimens treated by EP-USRP with optimized experimental parameters show a higher hardness and greater impact depth within the strengthened layer than that treated by USRP as depicted in Fig. 2(a). The nanoindentation hardness is maintained at 2.4 GPa in solution annealed specimens uniformly. After USRP and EP-USRP, there is a remarkable improvement in surface hardness for all specimens. For the USRP-treated specimen, hardness at the top surface is up to 5.8 GPa. In EP-USRP, the specimen treated at 600 Hz shows the highest hardness at the top surface of 6.7 GPa. But at a higher frequency of 650 Hz, the hardness at the top surface shows a lower value of 6.4 GPa. That means there is an optimal electropulsing parameter, and excessive current (650 Hz) may result in deterioration of the processing result in EP-USRP. Both in USRP and EP-USRP, significant work hardening induced by SPD based on the combination of dynamic impact superimposed on static extrusion can promote wear resistance and present a higher resistance to fatigue crack initiation dramatically.^{9,18}

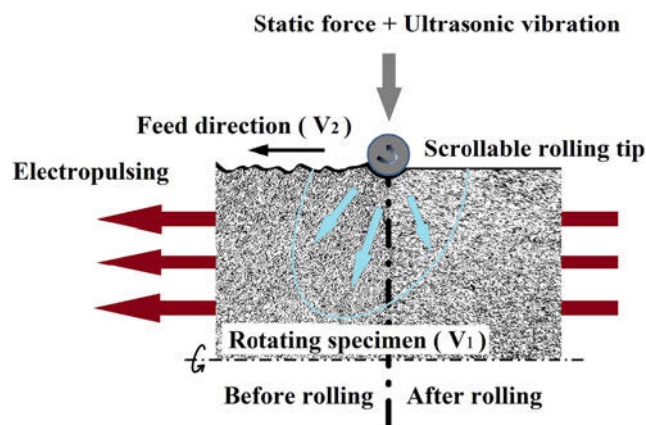


FIG. 1. Basic mechanism principle demonstration of EP-USRP. (Reproduced from Ref. 9. Mater. Sci. Eng., A, 2016).

TABLE II. Electropulsing parameters used in USRP and EP-USRP.

Sample number	Frequency (Hz)	Root-mean-square current density (A/mm^2)	Amplitude current density (A/mm^2)	Duration (μs)	Surface equilibrium temperature ($^{\circ}\text{C}$)
0	26
1	550	0.96	6.59	60	102
2	600	1.08	7.72	60	119
3	650	1.19	8.85	60	141

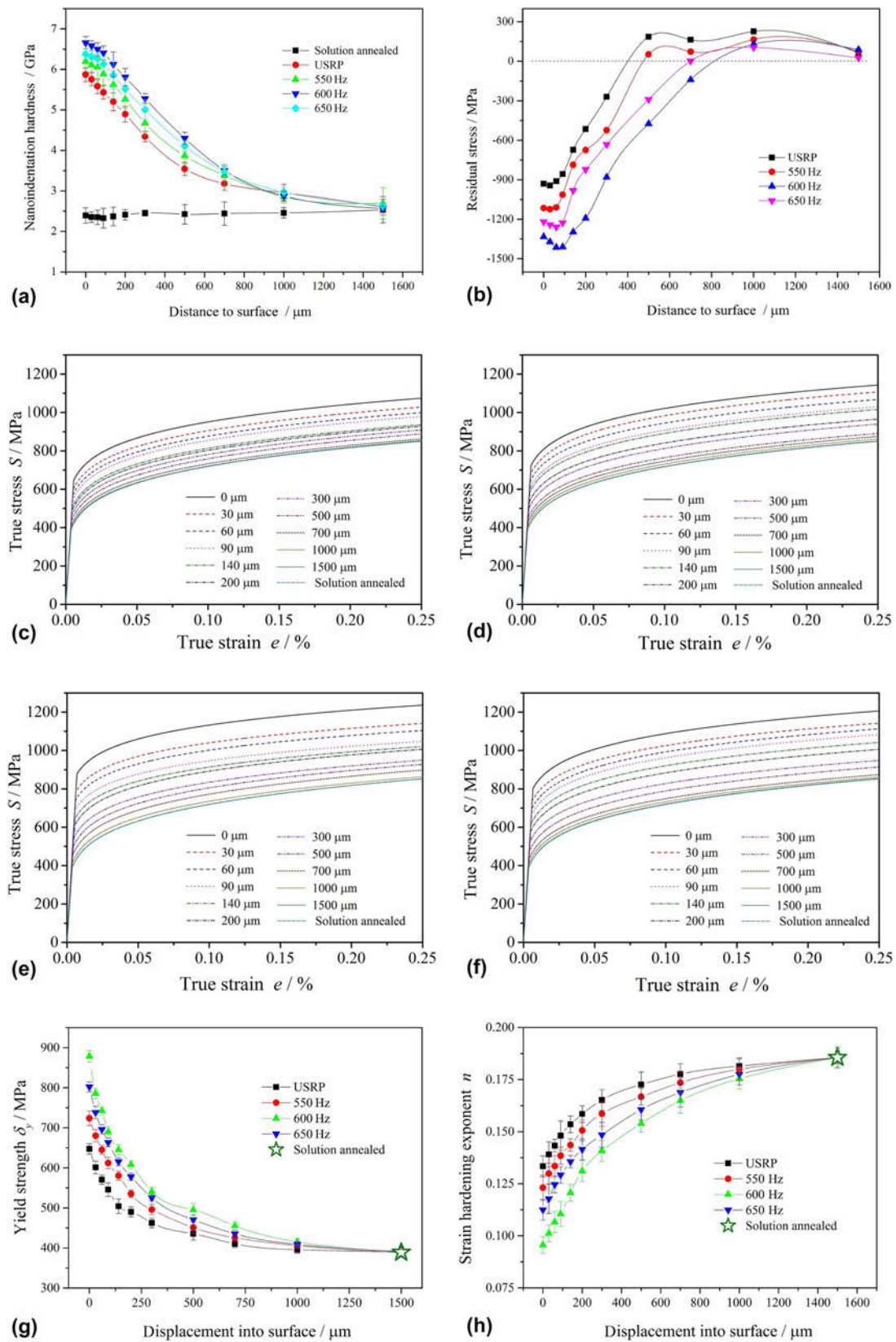


FIG. 2. Cross-sectional nanoindentation hardness (a), residual stress gradient distributions (b), in-depth true stress–true strain curves: USRP (c) and EP-USRP at 550 Hz (d), 600 Hz (e), and 650 Hz (f), and cross-sectional yield strength (g), and strain hardening exponent (h) gradient distribution within the strengthened layer.

Figure 2(b) shows the residual stress distribution within the strengthened layer induced by USRP and EP-USRP. Great residual compressive stress is produced from the top surface to a certain depth by processing. Deeper into inside, residual tensile stress begins to appear until the stress-free state of the matrix is reached instead of. The action depth of residual compressive stress for EP-USRP at 600 Hz is about 800 μm , but it is only 400 μm for USRP. Note that the maximum value of residual compressive stress is not at the top surface, but at the subsurface, about the depth of 50–100 μm . This is a typical characteristic of the in-depth residual stress distribution within the strengthened layer induced by SPD.¹⁹ For the specimen treated by EP-USRP at 600 Hz, the maximum residual compressive stress is -1414 MPa, significantly higher than -943 MPa of USRP. Greater residual compressive stress is very beneficial to the fatigue and wear resistance performance of the material, and it is of interest in the engineering application of the metallic component.^{4,5,18,20} Unfortunately, an evident stress release is presented at higher frequency (650 Hz) in EP-USRP, and the deterioration of the strengthening effect is brought out to a certain degree. It is implied that the optimized electro-pulsing parameters are very important in EP-USRP. The greater residual compressive stress within the strengthened layer induced by EP-USRP is related to the finer ultra-refined grains and the accelerated martensitic transformation caused by electropulsing, which will be discussed in detail later.

B. Evolution of cross-sectional true stress–true strain curve, yield strength, and strain hardening exponent within the strengthened layer

Based on material parameters and for diverse process parameters, the cross-sectional true stress–true strain curves, yield strength, and strain hardening exponent of treated specimens representing the power law relationship are shown in Figs. 2(c)–2(h). It can be seen that for all specimens after treatment, the strength property is presented with gradient distribution. The surface strength is the highest and gradually decreases with increasing depth. For USRP, the yield strength on the surface is 647.5 MPa, increasing from 390 MPa of solution annealed. For EP-USRP at 600 Hz, the yield strength on the surface is 878.4 MPa, the highest value in the present work. As depicted, the strain hardening exponent shows the opposite trend of yield strength. But like hardness, excessive current (650 Hz) may also result in deterioration. The gradient distribution of the surface mechanical properties is very beneficial for a good adhesion between the strengthened layer and the matrix.

C. Evolution of fatigue performance

Component fatigue performance affects its long-term stability in structural applications.^{18,21} As can be seen in

Fig. 3, the fatigue performance increased significantly after treated for all specimens, but there is a greater improvement in EP-USRP. For the USRP specimen, the average rotating bending fatigue strength is 561.5 MPa, which corresponds to 1.5 times improvement than 368.8 MPa of the specimen processed by mechanical polishing. In EP-USRP, the higher average fatigue strength, 593.5 MPa, is made dramatically. The plastically deformed surface results in high surface hardness [shown in Fig. 2(a)], which presents a higher resistance to crack initiation.¹⁸ In addition, the high magnitude of surface residual compressive stress [shown in Fig. 2(b)] also contributes to the improvement. During the fatigue test, the surface compressive residual stress can decrease the magnitude of the effective tensile stress and lead to improved fatigue strength.¹⁰ Thus, the fatigue performance improvement is the comprehensive effect of surface residual compressive stress, surface hardening, and microstructural changes.^{10,18,22}

SEM micrographs show big difference of fracture surfaces between the specimens treated by mechanical polishing, USRP, and EP-USRP, respectively. As depicted in Figs. 4(a), 4(b), and 4(g), typical fracture surface morphologies are presented for specimens treated by mechanical polishing and USRP, respectively. After fatigue tests, the specimens are completely fractured. The fracture surfaces are composed of fatigue source, crack growth zone, and transient fracture zone. Due to residual compressive stress, the fatigue source in USRP is at the subsurface, about 260 μm to the surface [Fig. 4(e)].¹⁰ But for the sample treated by mechanical polishing, it is located on the surface [Fig. 4(d)]. In other words, USRP causes the fatigue source to move inward. What is more noteworthy in the present work is that the abnormality of the fracture surface produced by EP-USRP. After fatigue tests and as shown in Fig. 4(g), all EP-USRP specimens are not completely fracture, but are still partially connected together. There are only fatigue source and crack growth zone on the fracture surface, no transient fracture zone exists [see Fig. 4(c), the shown manual fracture zone is generated by hand]. This incomplete fracture means a higher reservation of safety in practical engineering application. In addition, a greater fatigue source depth [about 360 μm , in Fig. 4(f)] is presented in EP-USRP because of a higher residual compressive stress than USRP. Beyond above, fatigue striations and fibrous stripes, which have been commonly observed in fatigue tests, also occurred in the fracture surface, as can be seen in Figs. 4(d), 4(e), and 4(f). Striations are fatigue features that indicate the position of the crack tip and are perpendicular to the stripes.²³ The radial fibrous stripes emanate from the crack initiation site and are consistent with crack growth path. In the propagation process of fatigue crack, height difference could exist between the different propagation paths resulting in laceration of the

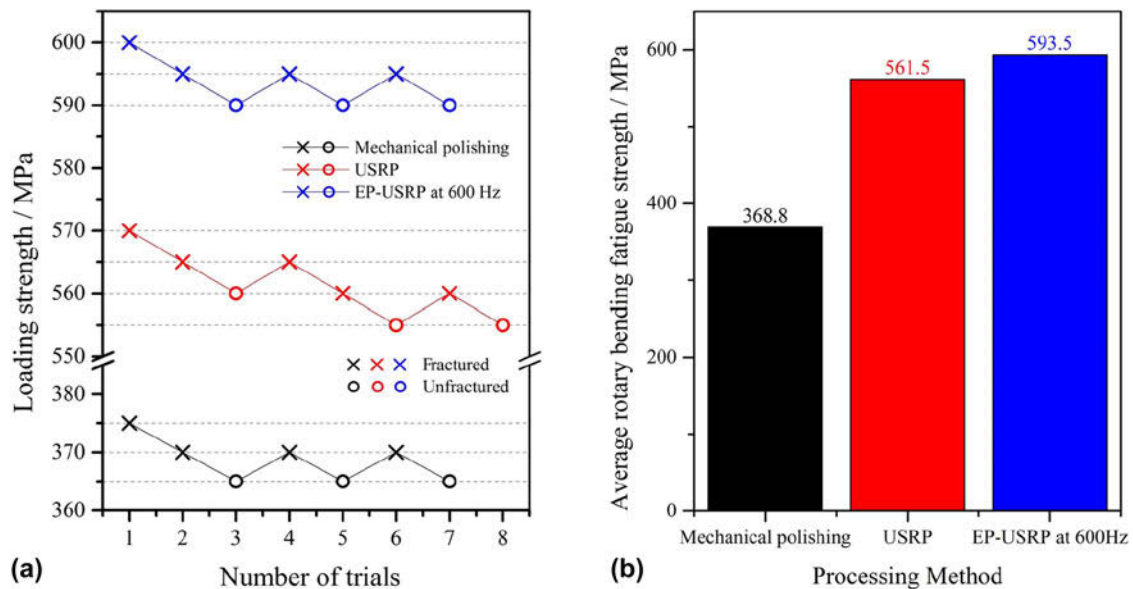


FIG. 3. Loading-failure up-and-down curves (a) and the average rotating fatigue strength (b) from the rotating bending fatigue test of the specimens processed by mechanical polishing, USRP, and EP-USRP at 600 Hz, respectively.

material and subsequent formation of fibrous stripes.^{23,24} But for the specimens treated by EP-USRP, the rapid propagation process of fatigue crack is prevented by the incomplete fracture zone after it passes through the crack growth zone. This is a good phenomenon for reservation of safety, and further study is needed to clarify this point.

IV. DISCUSSION

A. Evolution of microstructure and residual stress in the strengthened layer

As depicted in Fig. 5, cross-sectional SEM micrographs at 60 μm below the surface show the obvious difference between deformation microstructures induced by USRP and EP-USRP, respectively. There are a few of annealing twins in the solution annealed specimen [Fig. 5(a)]. After USRP, many deformation bands within grains appear, distributing in parallel unidirection and throughout the grain [Fig. 5(b)]. For EP-USRP at 550 Hz, the parallelism of deformation bands is destroyed, and interreaction between those deformation bands begins to appear [Fig. 5(c)]. The degree of this destruction aggravates with increasing frequency and reaches a maximum at 600 Hz, confirmed by many clustered microstructures [Fig. 5(d)]. However, at a higher frequency of 650 Hz, the clustered microstructures are weakened to some degree [Fig. 5(e)]. The difference of deformation microstructures indicates the change in the main mechanism of plastic deformation.⁹

In TEM micrographs and corresponding SADPs as shown in Fig. 6, deformation twins within the strengthened layer in USRP can be observed [Fig. 6(a)], the corresponding SADP [Fig. 6(b)] can prove that the

parallel deformation bands formed in USRP are deformation twins. In EP-USRP at 600 Hz, ultra-refined grains and more microstructures, such as dislocation cells and dislocation tangles, can be observed within the strengthened layer [Figs. 6(c) and 6(d)]. This indicates that a better reinforcement effect can be achieved by EP-USRP using the optimized parameters than USRP.

The morphology and distribution of grains described by EBSD IPFs and corresponding phase distribution within the strengthened layer are shown in Fig. 7. Coarse equiaxed annealed grains are observed in the solution annealed specimen, and the average size is about 15 μm [Fig. 7(a2)]. After USRP treatment, refined grains are generated in the surface layer within a depth range from surface to 40 μm [Fig. 7(b2)]. In EP-USRP, more ultra-refined grains are observed, and greater distribution depths are reached than USRP [Figs. 7(c2), 7(d2), and 7(e2)]. Corresponding magnified images in the top strengthened layer [Figs. 7(a1), 7(b1), 7(c1), 7(d1), and 7(e1)] show the micromorphology of the ultra-refined grains. As shown in figures, the enhancement effect is the best at 600 Hz in EP-USRP. The ultra-refined grains facilitate the enhancement of hardness and wear resistance. Phase transformation from austenite to martensite induced by SPD is an important characteristic in the plastic processing of AISI 304 stainless steel.^{25–27} The process of this change is described in detail by EBSD. The solution annealed AISI 304 stainless steel is almost entirely composed of austenite [Fig. 7(a3)]. When it is subjected to SPD in USRP, a remarkable phase deformation from γ -austenite to α' -martensite within the surface layer can be observed [Fig. 7(b3)]. It is worth noting that in EP-USRP comparatively, the martensite

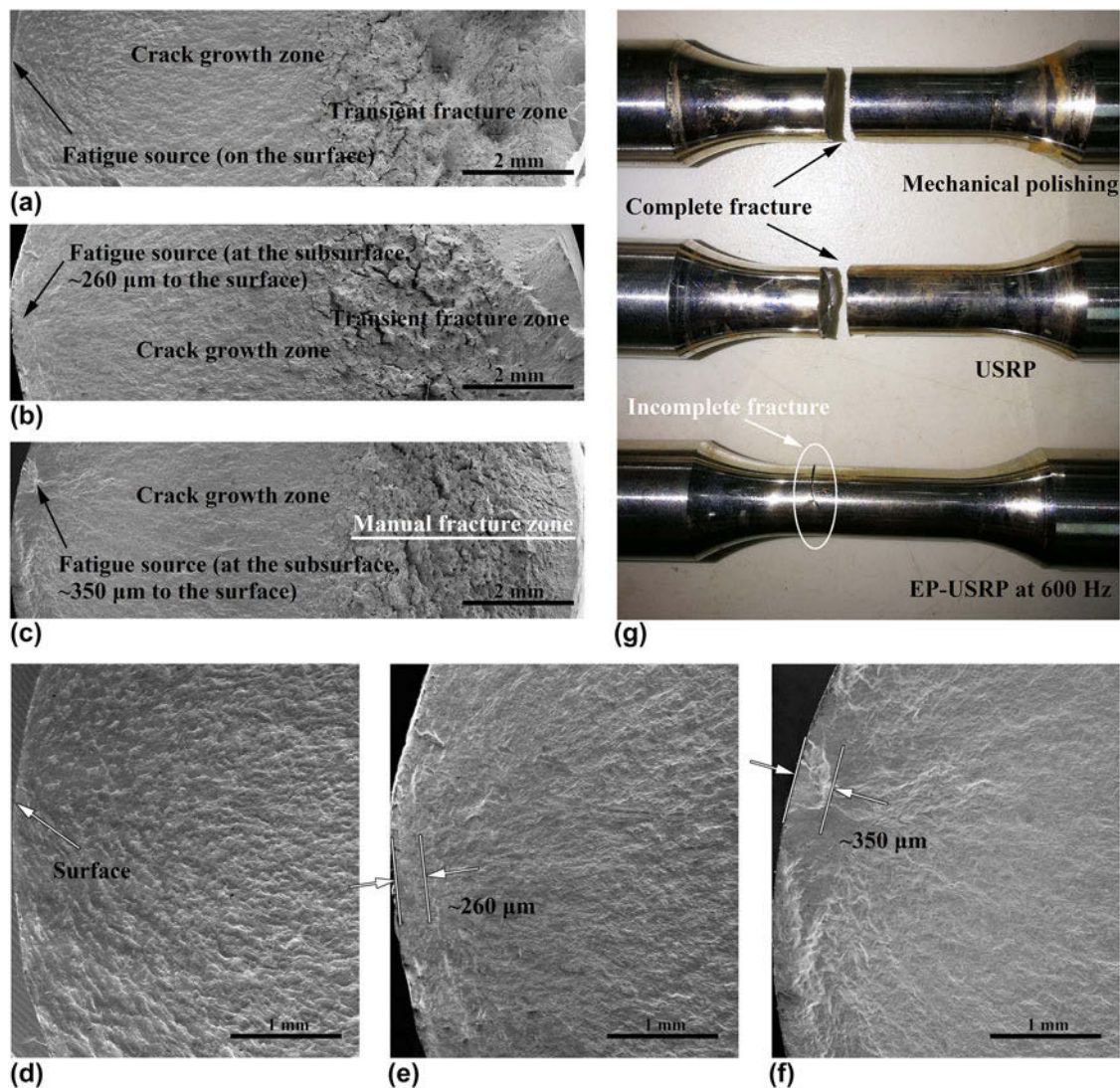


FIG. 4. SEM micrographs of fracture surfaces of mechanical polishing (a), USRP (b) and EP-USRP at 600 Hz (c), corresponding magnified images of the fatigue source zones (d), (e), and (f), and the physical photo of the fatigue tested specimens (g).

volume fraction in the strengthened layer increases when electropulsing is applied [Figs. 7(c3), 7(d3), and 7(e3)]. At 600 Hz, the volume fraction is significantly higher than that of USRP; i.e., the martensitic phase transformation is accelerated by electropulsing.⁹ But at a higher frequency of 650 Hz, the volume fraction begins to decrease due to excessive current. Owing to its high hardness, the transformed martensitic phase in return can impact the surface mechanical properties significantly, such as higher surface hardness and greater wear resistance.

Structure strengthening and stress strengthening are two important strengthening mechanisms in plastic deformation processing based on SPD for metallic materials.¹⁰ Structure strengthening refers to the improvement in the properties of a material as a result of changes in the microstructure, such as refined grains, pileups of

dislocations, phase transformation, second phase, and so on. The modified microstructure of a metal can improve the hardness, wear resistance, and fatigue performance significantly.

During the plastic deformation of metal materials, dislocation slip and deformation twinning are two competing processes.¹⁸ For AISI 304 stainless steel during the traditional plastic deformation process, deformation twinning plays an important role because of its relatively low stacking fault energy (SFE).^{18,28–30} From the principle of plastic deformation, it can be stated that the lower the SFE, the higher the appearance probability of stacking faults and the wider the extended width of the stacking faults. Because of great difficulty in concentrating for a widely separated partial dislocation, it is very unlikely to cross-slipping between the different glide planes in the form of a perfect dislocation. In this case, planar

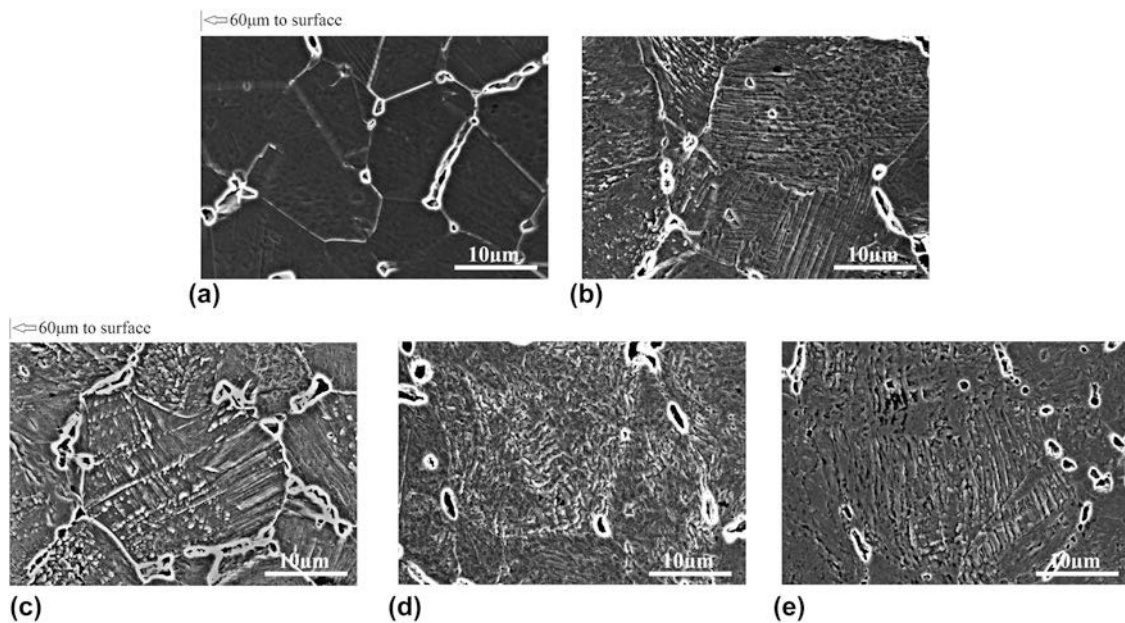


FIG. 5. Cross-sectional SEM micrographs showing the microstructural evolution within the strengthened layer: solution annealed (a), USRP (b) and EP-USRP at 550 Hz (c), 600 Hz (d), and 650 Hz (e) (the left edge of each figure is the material surface).

dislocation arrays and stacking faults with widely separated partial dislocations are more easily formed on the same $\{111\}$ slip planes in AISI 304 stainless steel.^{28,31} The extended dislocations' accumulation above from the plastic strain leads to stress concentration, which is favorable for the nucleation of deformation twins. Then the deformation twinning may occur when critical twinning stress is met.²⁸ Therefore, many parallel deformation bands are formed within the strengthened layer in USRP. As more plastic strain accumulates, deformation twins in different directions divide the grains into smaller sections, which eventually lead to refined grains.¹⁸ Meanwhile, the intersections of the stacking faults and twins generate plastic strain concentration, and those intersections serve as embryos for martensite formation. The martensite embryos then grow to refined crystallites when the material is subjected to further plastic strain. Finally, the refined grains and new martensite phase are obtained.^{7,9,18,28,29,32} The obtained martensite has a higher hardness and a bigger volume than primary austenite, which leads to a compressive stress. As a result, higher surface hardness, greater wear resistance, and higher residual compressive stress than the solution annealed are produced by USRP.

When electropulsing applied in EP-USRP, the SFE of AISI 304 stainless steel is enhanced rapidly due to the thermal and athermal effects of electropulsing.^{9,33,34} The SFE of metallic materials is mainly affected by temperature, components, segregation of the alloying element in stacking faults, etc. The segregation of the alloying element in stacking faults shows a strong pinning effect on the concentration and movement of the extended

dislocation before transforming to a perfect dislocation and then completing a cross slip. Like the Joule heating effect, the athermal effect of electropulsing can speed up the diffusion of atoms and the movement of dislocations in the material significantly. The increase in diffusion speed of the alloying element in stacking faults is conducive to the reduction of the above-mentioned pinning effect. Therefore, the concentration and movement of the extended dislocation are more easily to happen, and the extended dislocation can probably transform to a perfect dislocation and then glide to another glide plane and complete a cross slip, which is accompanied by suppressed deformation twinning.³⁵ Thus, dislocation cells and dislocation tangles can form through dislocation cross slip, and plastic strain concentration is produced. In the subsequent processing, these dislocation cells and dislocation tangles grow into the new refined grains, and the martensite phase transformation is completed.⁹ Therefore, there is an entirely different mechanism of plastic deformation between USRP and EP-USRP. But what is more noteworthy in EP-USRP is the further modified microstructure and performance than USRP that are induced by electropulsing. Electropulsing can accelerate the mobility of dislocation in plastic deformation.³⁶⁻⁴¹ Therefore, much easier cross slip for dislocations can be carried out, and more dislocation cells and dislocation tangles can form in the same time and space. That means the growing space for every dislocation cell or dislocation tangle is very small. Therefore, the squeeze effect between the new generated martensite grains is dramatically magnified because of the dilatational volume expansion from austenite to martensite. In

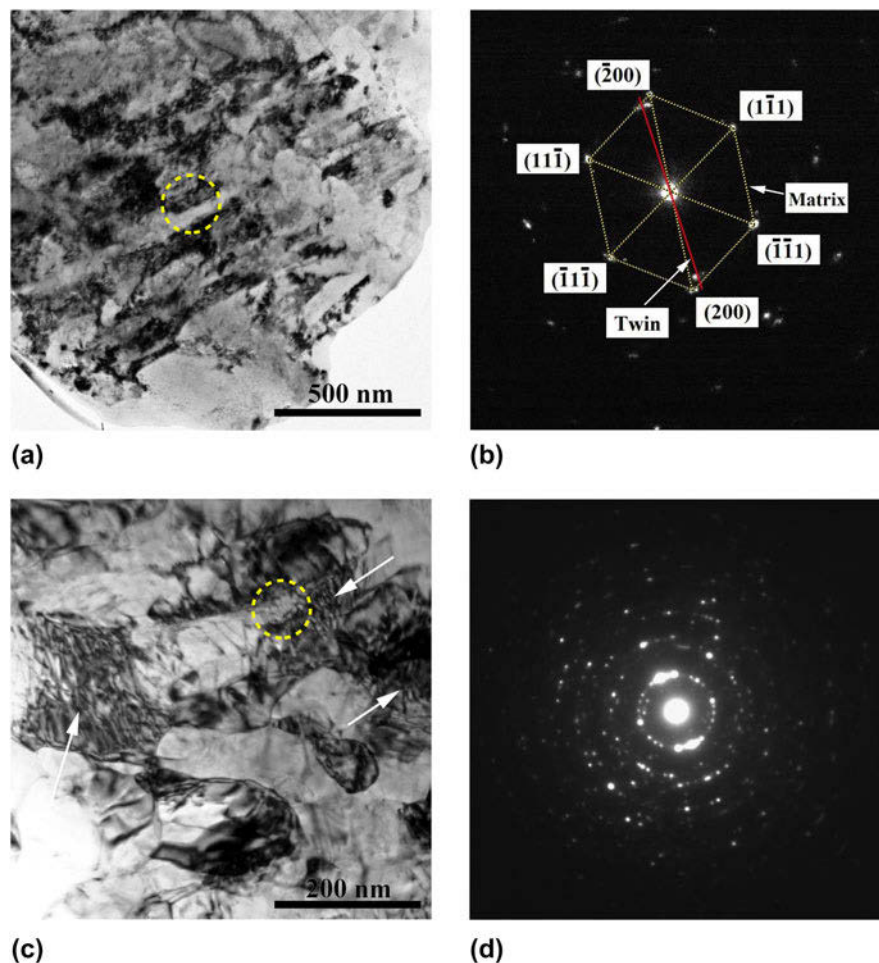


FIG. 6. TEM images and corresponding SADPs at 30 μm below the surface showing: (a) highly dense deformation twins induced by USRP and (b) diffraction pattern taken from the dotted ring in (a) revealing reflections at $1/3\{110\}$ positions from the deformation twins, (c) highly dense dislocations (shown by arrows) induced by EP-USRP at 600 Hz, and (d) diffraction pattern taken from the dotted ring in (c) revealing the refined grains.

addition, more dramatic lattice distortion is caused by enhanced plastic deformation within the surface layer by electropulsing. Thus compared with USRP, finer ultra-refined grains and more stronger residual compressive stress due to excessive extrusion between each martensite grain are generated in EP-USRP.^{9,37}

In addition, the change of material system free energy and enhanced stability of ultra-refined grain boundaries induced by electropulsing are non-negligible reasons for the improvement of material performance brought by EP-USRP. Plastic deformation inducing processes like rolling or drawing may introduce grain boundaries into metals and refined grains; yet in most metals, this refinement saturates at the submicrometer scale due to grain boundary annihilation above a threshold level of strain.^{42,43} But when electropulsing is applied to the material, electric current free energy, which is different from the chemical free energy, is introduced into the system as an extra free energy term.⁴⁴ Electric current

free energy is dependent on the microstructure configuration. And the refinement of grains can cause the electric current free energy to reduce in some cases. This compensates the increment of interfacial free energy during refining and enables the processing to achieve finer microstructure^{44,45}; i.e., finer ultra-refined grains can be generated. Therefore, electropulsing in EP-USRP can break the grain refining limit that is induced by SPD drastically. On the other hand, some metals at some grain sizes in the nanometer regime often become more and more soft with decreasing grain sizes, opposing with the classical Hall–Petch relationship.^{46–48} Hall–Petch relationship, the increase in strength is inversely proportional to the square root of grain size, is established with the strengthening mechanism based on dislocation pileups at grain boundaries, which hinder dislocation motion. Grain size reduction into the nanometer scale, i.e., with higher density of grain boundaries, can make dislocation pileup difficult, raise into question continued hardening.^{49,50} But

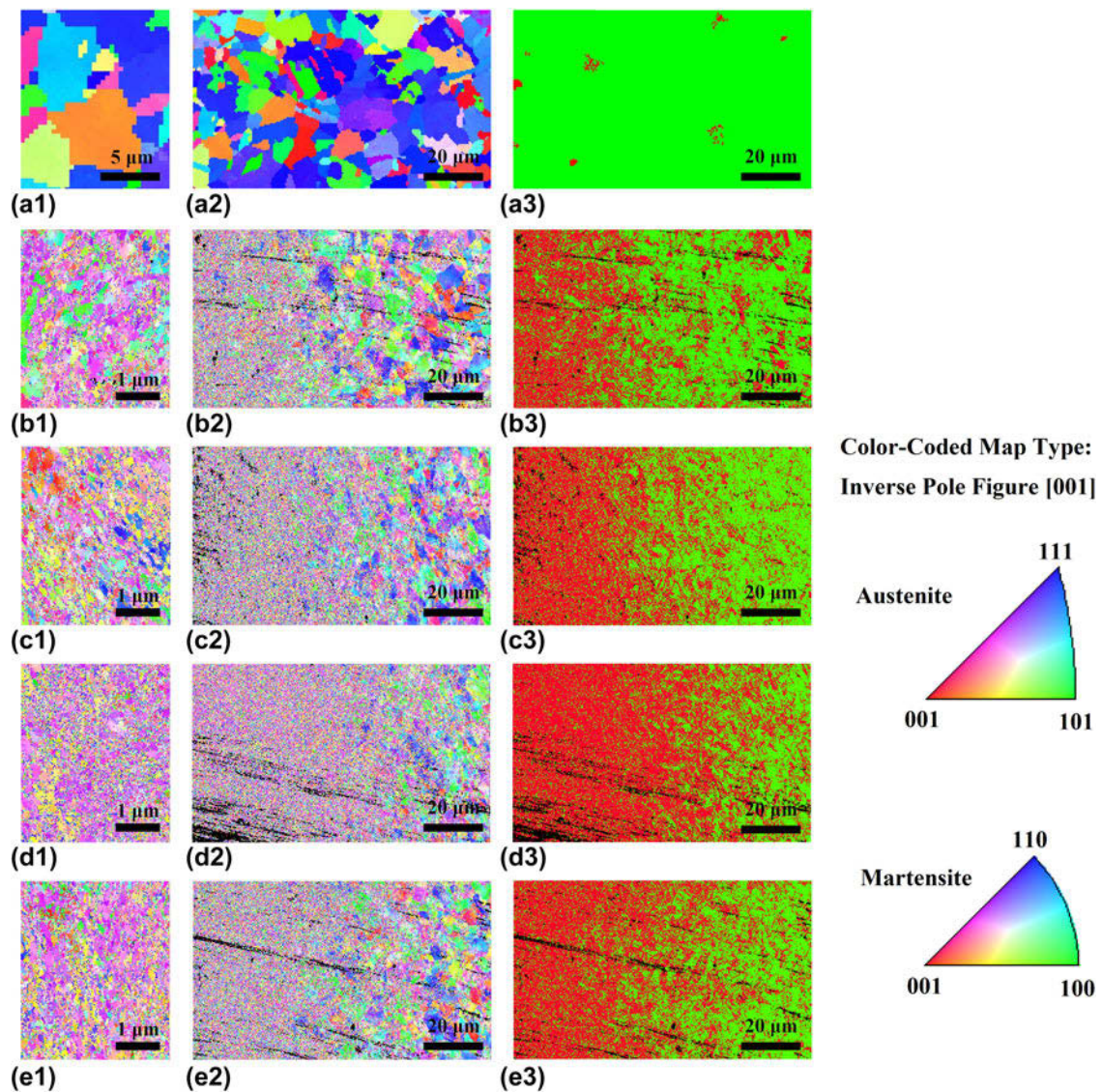


FIG. 7. EBSD IPFs within the strengthened layer: solution annealed (a2), USRP (b2), and EP-USRP at 550 Hz (c2), 600 Hz (d2), and 650 Hz (e2), and corresponding magnified images within the top strengthened layer: solution annealed (a1), USRP (b1), and EP-USRP at 550 Hz (c1), 600 Hz (d1), and 650 Hz (e1), and corresponding phase distribution within the strengthened layer (martensite represented by red and austenite represented by green): solution annealed (a3), USRP (b3), and EP-USRP at 550 Hz (c3), 600 Hz (d3), and 650 Hz (e3) (the left edge of each figure is the material surface).

in metals with extremely fine grains, the stability of grain boundaries plays a crucial role in determining the plastic deformation and hardness. For grain boundaries with a low stability against plastic straining, deformation mechanism shifts from full dislocation slip to grain boundary-mediated process at a critical grain size.⁴⁶ And this anomaly may lead to a lower hardness in a metal that with ultrafine grains; i.e., it is not advisable to pursue the superfining of grains purely and blindly in strengthen processing based on plastic deformation for metallic materials. But fortunately, electropulsing applied in EP-USRP can eliminate this disadvantage dramatically by effective stabilization of high angle grain boundaries that

exists in nanosized grains and shows lower thermal and mechanical stability⁵¹ through grain boundary relaxation,⁵² grain boundary segregation of solute atoms,^{53,54} or both processes.⁴⁶ The thermal and athermal effects of electropulsing can effectively promote the diffusion and redistribution of solute atoms within grains and on grain boundaries.^{36,38,45} These effects are equivalent to a moderate annealing at modest temperatures but without obvious grain size change.⁴⁶ Electropulsing can also induce some beneficial elements' enrichment at grain boundaries, and the segregation of the solute atoms or existed impurity atoms at grain boundaries may also be induced. The enrichment and segregation can increase the

stability of grain boundaries significantly, which facilitates structural refinement down to the nanoscale.^{42,46} Therefore, in the following processing, ultrafine grains show a stronger resistance to plastic deformation due to more stable grain boundaries and present a higher hardness finally. Besides accelerated martensite transformation and gradient distribution of finer grains and interfaces with spacing ranging from the nanoscale to macroscale are effective strategy for strain delocalization,⁵¹ remarkable improvement homogeneity in plastic deformation based on dislocation slipping induced by electropulsing is also beneficial for fatigue performance.⁵⁵ Under the combined effect of the above factors, fatigue performance is improved significantly, while friction coefficient and wear amount are reduced dramatically.^{9,42,43,46}

Stress strengthening is another important intrinsic mechanism for the improvement of the fatigue performance induced by USRP, and it has been considered to play a leading role on fatigue performance all the time.^{10,56} In the plastic deformation process, lattice distortion caused by external force is an important cause of internal residual compressive stress. Another important reason for residual compressive stress is the squeeze effect between the new generated and refined martensite grains because of the dilatational volume expansion from austenite to martensite. Great residual compressive stress induced by nonuniform surface cyclic plastic deformation and inflated transformational martensite phase presents a high resistance to crack initiation and decreases the magnitude of the effective tensile stress.¹⁸ So that the fatigue resistance can be improved. Because of the nonmonotonic distribution of residual stress in the strengthened layer, the amplitude of effective destructive stress exerted on the material is not on the surface, but at

the subsurface. That is the reason why the fatigue source shifts to the subsurface in the fatigue testing specimen treated by USRP from that treated by mechanical polishing. With the help of electropulsing in EP-USRP, greater residual compressive stress induced by deteriorated SPD, finer grains and accelerated martensite phase transformation than that in USRP further decreases the magnitude of the effective tensile stress and shows a stronger resistance to crack initiation. Therefore, better fatigue performance is presented by EP-USRP. In addition, crack healing and tip passivating induced by electropulsing in EP-USRP are other two important factors for the stronger resistance to crack initiation, and they are reflected in the dramatic improvement of fatigue performance ultimately.^{8,9,57,58}

B. Illumination of the mechanism on the fatigue performance evolution under the action of EP-USRP

The fatigue performance evolution of AISI 304 stainless steel induced by EP-USRP is depicted in Fig. 8. For the mechanical polished fatigue specimen, there are a lot of microcracks on the surface, even though there is a good finish on the macro. Under the action of alternating load, fatigue source originates from the surface based on the existed microcrack, following by crack growth and transient fracture. Finally, the conventional fatigue strength and fracture morphology are presented as shown in Figs. 4(a), 4(d), and 4(g).

In USRP, refined grains and residual compressive stress can be generated at and below the material surface to a certain depth. At the same time, a surface with lower roughness is presented because of the rolling effect. Then the structure strengthening and stress strengthening are

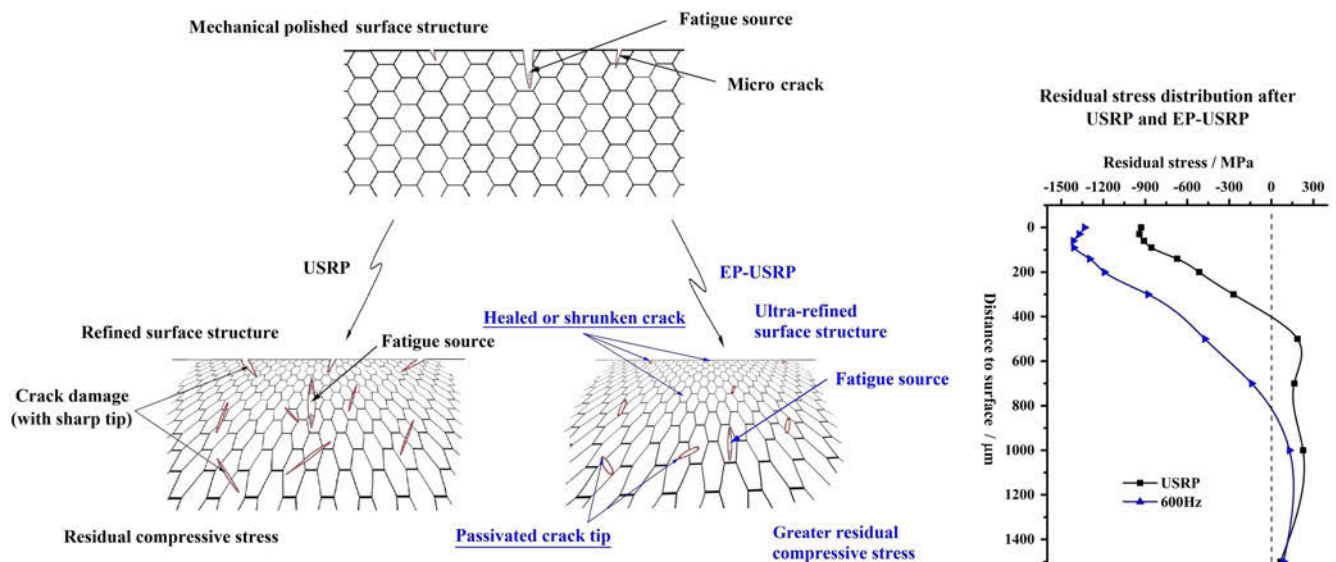


FIG. 8. Schematic illumination showing the fatigue performance evolution of AISI 304 stainless steel under the action of EP-USRP.

introduced into the surface of the material. Surface mechanical properties, such as hardness and wear resistance, are enhanced significantly. Meanwhile, high surface hardness shows a high resistance to fatigue crack initiation. In the fatigue test, the residual compressive stress can decrease the magnitude of the effective tensile stress. Thus, an obvious improvement of fatigue performance is made by USRP. But because of the non-monotonic distribution of residual stress in the strengthened layer, the amplitude of effective destructive stress exerted on the material is not on the surface, but at the subsurface. Also due to SPD, a large number of microdefects, such as microcracks with sharp tips, are created at the subsurface. Therefore, the fatigue source originates from the microcrack that locates at the subsurface where effective destructive stress shows a higher value and obvious fragility of the material is presented. As result, a high fatigue strength is achieved, and as depicted in Figs. 4(b), 4(e), and 4(g), and the fracture morphology with moving inward fatigue source is presented in USRP.

When electropulsing applied in EP-USRP, finer grains, higher surface hardness, greater residual compressive stress and more martensite than that generated by USRP are presented due to the comprehensive effect of elevated SFE, accelerated dislocation mobility, introduction of electric current free energy, and enhanced stability of ultra-refined grain boundary as discussed above. Crack healing and tip passivating rapidly occur at and below the surface, and the microdefects induced by SPD largely weakened and reduced. Meanwhile, significant improved homogeneity in plastic deformation based on dislocation slipping is induced by electropulsing. Higher surface hardness, finer ultra-refined grains, lots of grain boundaries, greater residual compressive stress, passivated crack tip, and preferable homogeneity in plastic deformation make the fatigue crack initiation more difficult. Therefore, the amplitude of effective destructive stress decreases further, and fatigue source moves to the deeper subsurface than that in USRP. In the fatigue test, crack growth is stopped at the transient fracture zone after crack initiating and passing through the growth zone because of insufficient driving force for crack growing. Therefore, a higher fatigue strength and an incomplete fracture morphology are presented as depicted in Figs. 4(c), 4(f), and 4(g). Finally, a dramatical improvement of fatigue performance brought by EP-USRP is achieved miraculously, and it shows very high reservation of safety for engineering application.

V. CONCLUSION

Compared with USRP, further modified structure strengthening and stress strengthening are generated within the surface strengthened layer by EP-USRP.

For AISI 304 stainless steel, the fatigue performance shows a higher average rotating bending fatigue strength. Anomalously and noteworthy, higher reservation of safety, manifested as an incomplete fracture, is a valuable feature property for the specimens treated by EP-USRP in practical engineering applications. In EP-USRP, higher surface hardness, effective crack healing, finer ultra-refined grains, and greater residual compressive stress than that induced by USRP within the surface strengthened layer are likely the primary intrinsic reasons for the remarkable improvement of fatigue performance.

ACKNOWLEDGMENT

This work was supported by the project funded by China Postdoctoral Science Foundation (No. 2017M620770) and Shenzhen Development & Reform Commission Engineering Laboratory Project (Shenzhen development & Reform 2015-1033).

REFERENCES

1. A.J. Sterling, B. Torries, N. Shamsaei, S.M. Thompson, and D.W. Seely: Fatigue behavior and failure mechanisms of direct laser deposited Ti-6Al-4V. *Mater. Sci. Eng., A* **655**, 100 (2016).
2. H. Wang, G. Song, and G. Tang: Evolution of surface mechanical properties and microstructure of Ti-6Al-4V alloy induced by electropulsing-assisted ultrasonic surface rolling process. *J. Alloys Compd.* **681**, 146 (2016).
3. K. Shibanuma, K. Ueda, H. Ito, Y. Nemoto, M. Kinefuchi, K. Suzuki, and M. Enoki: Model for predicting fatigue life and limit of steels based on micromechanics of small crack growth. *Mater. Des.* **139**, 269 (2018).
4. S. Taheri, L. Vincent, and J-C. Le-Roux: Classification of metallic alloys for fatigue damage accumulation: A conservative model under strain control for 304 stainless steels. *Int. J. Fatigue* **70**, 73 (2015).
5. Y. Bai, M. Akita, Y. Uematsu, T. Kakiuchi, Y. Nakamura, and M. Nakajima: Improvement of fatigue properties in type 304 stainless steel by annealing treatment in nitrogen gas. *Mater. Sci. Eng., A* **607**, 578 (2014).
6. M. Boeff, H. ul Hassan, and A. Hartmaier: Micromechanical modeling of fatigue crack initiation in polycrystals. *J. Mater. Res.* **32**, 4375 (2017).
7. Q-q. Duan, B. Wang, P. Zhang, K. Yang, and Z-F. Zhang: Improvement of notch fatigue properties of ultra-high CM400 maraging steel through shot peening. *J. Mater. Res.* **32**, 4424 (2017).
8. H. Wang, G. Song, and G. Tang: Enhanced surface properties of austenitic stainless steel by electropulsing-assisted ultrasonic surface rolling process. *Surf. Coat. Technol.* **282**, 149 (2015).
9. H. Wang, G. Song, and G. Tang: Effect of electropulsing on surface mechanical properties and microstructure of AISI 304 stainless steel during ultrasonic surface rolling process. *Mater. Sci. Eng., A* **662**, 456 (2016).
10. R. Wang and J. Ru: Overall evaluation of the effect of residual stress induced by shot peening in the improvement of fatigue fracture resistance for metallic materials. *Chin. J. Mech. Eng.* **28**, 416 (2015).

11. S. Suresh and A.E. Giannakopoulos: A new method for estimating residual stresses by instrumented sharp indentation. *Acta Mater.* **46**, 5755 (1998).
12. A.C. Fischer-Cripps: A review of analysis methods for sub-micron indentation testing. *Vacuum* **58**, 569 (2000).
13. L.M. Farrissey and P.E. McHugh: Determination of elastic and plastic material properties using indentation: Development of method and application to a thin surface coating. *Mater. Sci. Eng., A* **399**, 254 (2005).
14. N. Ogasawara, N. Chiba, and X. Chen: Measuring the plastic properties of bulk materials by single indentation test. *Scr. Mater.* **54**, 65 (2006).
15. H. Lan and T.A. Venkatesh: Determination of the elastic and plastic properties of materials through instrumented indentation with reduced sensitivity. *Acta Mater.* **55**, 2025 (2007).
16. Y. Liu, X. Zhao, and D. Wang: Determination of the plastic properties of materials treated by ultrasonic surface rolling process through instrumented indentation. *Mater. Sci. Eng., A* **600**, 21 (2014).
17. M. Dao, N. Chollacoop, K.J. Van Vliet, T.A. Venkatesh, and S. Suresh: Computational modeling of the forward and reverse problems in instrumented sharp indentation. *Acta Mater.* **49**, 3899 (2001).
18. Y. Chang, A. Telang, A.S. Gill, S. Suslov, Y. Idell, K. Zwiackier, J.M.K. Wiezorek, Z. Zhong, Q. Dong, S.R. Mannava, and V.K. Vasudevan: Gradient nanostructure and residual stresses induced by ultrasonic nano-crystal surface modification in 304 austenitic stainless steel for high strength and high ductility. *Mater. Sci. Eng., A* **613**, 274 (2014).
19. X. Yang, J. Zhou, and X. Ling: Study on plastic damage of AISI 304 stainless steel induced by ultrasonic impact treatment. *Mater. Des.* **36**, 477 (2012).
20. I. Nikitin and M. Besel: Correlation between residual stress and plastic strain amplitude during low cycle fatigue of mechanically surface treated austenitic stainless steel AISI 304 and ferritic-pearlitic steel SAE 1045. *Mater. Sci. Eng., A* **491**, 297 (2008).
21. N.T. Aboulkhair, I. Maskery, C. Tuck, I. Ashcroft, and N.M. Everitt: Improving the fatigue behaviour of a selectively laser melted aluminium alloy: Influence of heat treatment and surface quality. *Mater. Des.* **104**, 174 (2016).
22. L. Yang, N.R. Tao, K. Lu, and L. Lu: Enhanced fatigue resistance of Cu with a gradient nanograined surface layer. *Scr. Mater.* **68**, 801 (2013).
23. G.J. Deng, S.T. Tu, Q.Q. Wang, X.C. Zhang, and F.Z. Xuan: Small fatigue crack growth mechanisms of 304 stainless steel under different stress levels. *Int. J. Fatigue* **64**, 14 (2014).
24. M. Kimura, K. Yamaguchi, M. Hayakawa, K. Kobayashi, S. Matsuoka, and E. Takeuchi: Fatigue fracture mechanism maps for a type 304 stainless steel. *Metall. Mater. Trans. A* **35A**, 1311 (2004).
25. A.Y. Chen, H.H. Ruan, J. Wang, H.L. Chan, Q. Wang, Q. Li, and J. Lu: The influence of strain rate on the microstructure transition of 304 stainless steel. *Acta Mater.* **59**, 3697 (2011).
26. C. Ye, S. Suslov, D. Lin, and G.J. Cheng: Deformation-induced martensite and nanotwins by cryogenic laser shock peening of AISI 304 stainless steel and the effects on mechanical properties. *Philos. Mag.* **92**, 1369 (2012).
27. J. Fan and T. Fu: Toughened austenitic stainless steel by surface severe plastic deformation. *Mater. Sci. Eng., A* **552**, 359 (2012).
28. H.W. Zhang, G. Liu, Z.K. Hei, J. Lu, and K. Lu: Martensitic phase transformation induced by surface mechanical attrition treatment—II. Grain refinement mechanism. *Acta Metall. Sin.* **39**, 347 (2003).
29. H.W. Zhang, Z.K. Hei, G. Liu, J. Lu, and K. Lu: Formation of nanostructured surface layer on AISI 304 stainless steel by means of surface mechanical attrition treatment. *Acta Mater.* **51**, 1871 (2003).
30. K. Wang, N.R. Tao, G. Liu, J. Lu, and K. Lu: Plastic strain-induced grain refinement at the nanometer scale in copper. *Acta Mater.* **54**, 5281 (2006).
31. K. Lu and J. Lu: Nanostructured surface layer on metallic materials induced by surface mechanical attrition treatment. *Mater. Sci. Eng., A* **375**, 38 (2004).
32. D. Kulawinski, M. Hoffmann, T. Lippmann, G. Lamprecht, A. Weidner, S. Henkel, and H. Biermann: Isothermal and thermo-mechanical fatigue behavior of 16Mo3 steel coated with high-velocity oxy-fuel sprayed nickel-base alloy under uniaxial as well as biaxial-planar loading. *J. Mater. Res.* **32**, 4411 (2017).
33. L. Remy and A. Pineau: Temperature-dependence of stacking-fault energy in close-packed metals and alloys. *Mater. Sci. Eng.* **36**, 47 (1978).
34. K. Ishida: Direct estimation of stacking-fault energy by thermodynamic analysis. *Phys. Status Solidi A* **36**, 717 (1976).
35. H. Conrad, N. Karam, and S. Mannan: Effect of electric-current pulses on the recrystallization of copper. *Scr. Metall.* **17**, 411 (1983).
36. V.E. Gromov, Y.F. Ivanov, O.A. Stolboushkina, and S.V. Konovalov: Dislocation substructure evolution on Al creep under the action of the weak electric potential. *Mater. Sci. Eng., A* **527**, 858 (2010).
37. Y. Zhao, B. Ma, H. Guo, J. Ma, Q. Yang, and J. Song: Electropulsing strengthened 2 GPa boron steel with good ductility. *Mater. Des.* **43**, 195 (2013).
38. R.S. Qin, A. Rahnama, W.J. Lu, X.F. Zhang, and B. Elliott-Bowman: Electropulsed steels. *Mater. Sci. Technol.* **30**, 1040 (2014).
39. A. Rahnama and R.S. Qin: Electropulse-induced microstructural evolution in a ferritic-pearlitic 0.14% C steel. *Scr. Mater.* **96**, 17 (2015).
40. A. Rahnama and R.S. Qin: The effect of electropulsing on the interlamellar spacing and mechanical properties of a hot-rolled 0.14% carbon steel. *Mater. Sci. Eng., A* **627**, 145 (2015).
41. K.V. Sosnin, Y.F. Ivanov, V.E. Gromov, E.A. Budovskikh, and D.A. Romanov: Structure and properties of surface layers obtained due to titanium-surface alloying by yttrium via combined electron-ion-plasma treatment. *J. Surf. Invest.: X-Ray, Synchrotron Neutron Tech.* **8**, 1286 (2014).
42. X. Li and K. Lu: Playing with defects in metals. *Nat. Mater.* **16**, 700 (2017).
43. X.C. Liu, H.W. Zhang, and K. Lu: Strain-induced ultrahard and ultrastable nanolaminated structure in nickel. *Science* **342**, 337 (2013).
44. R. Qin: Using electric current to surpass the microstructure breakup limit. *Sci. Rep.* **7**, 41451 (2017).
45. R.S. Qin and A. Bhowmik: Computational thermodynamics in electric current metallurgy. *Mater. Sci. Technol.* **31**, 1560 (2015).
46. J. Hu, Y.N. Shi, X. Sauvage, G. Sha, and K. Lu: Grain boundary stability governs hardening and softening in extremely fine nanograined metals. *Science* **355**, 1292 (2017).
47. M.A. Meyers, A. Mishra, and D.J. Benson: Mechanical properties of nanocrystalline materials. *Prog. Mater. Sci.* **51**, 427 (2006).
48. A.J. Detor and C.A. Schuh: Tailoring and patterning the grain size of nanocrystalline alloys. *Acta Mater.* **55**, 371 (2007).
49. N.J. Petch: The cleavage strength of polycrystals. *J. Iron Steel Inst.* **174**, 25 (1953).

50. E.O. Hall: The deformation and ageing of mild steel. III. Discussion of results. *Proc. Phys. Soc., London, Sect. B* **64**, 747 (1951).
51. K. Lu: Stabilizing nanostructures in metals using grain and twin boundary architectures. *Nat. Rev. Mater.* **1**, 10619 (2016).
52. A. Hasnaoui, H. Van Swygenhoven, and P.M. Derlet: On non-equilibrium grain boundaries and their effect on thermal and mechanical behaviour: A molecular dynamics computer simulation. *Acta Mater.* **50**, 3927 (2002).
53. J. Weissmuller: Alloy effects in nanostructures. *Nanostruct. Mater.* **3**, 261 (1993).
54. R. Kirchheim: Grain coarsening inhibited by solute segregation. *Acta Mater.* **50**, 413 (2002).
55. H. Conrad, J. White, W.D. Cao, X.P. Lu, and A.F. Sprecher: Effect of electric-current pulses on fatigue characteristics of polycrystalline copper. *Mater. Sci. Eng., A* **145**, 1 (1991).
56. G.C. Bird and D. Saynor: The effect of peening-shot size on the performance of carbon-steel springs. *J. Mech. Work. Technol.* **10**, 175 (1984).
57. Y.Z. Zhou, J.D. Guo, M. Gao, and G.H. He: Crack healing in a steel by using electropulsing technique. *Mater. Lett.* **58**, 1732 (2004).
58. T. Yu, D. Deng, G. Wang, and H. Zhang: Crack healing in SUS304 stainless steel by electropulsing treatment. *J. Cleaner Prod.* **113**, 989 (2016).